

# Three-dimensional birefringence imaging with a microscope tilting stage. II. Biaxial crystals

L. A. Pajdzik and A. M. Glazer\*

Received 6 July 2006

Accepted 29 September 2006

 Physics Department, University of Oxford, Parks Road, Oxford OX1 3PU, UK. Correspondence  
 e-mail: glazer@physics.ox.ac.uk

The technique enables precise three-dimensional birefringence information of optically biaxial materials to be obtained. Equations derived here describe a mathematical model of the tilting-stage system for such crystals in any general orientation. This leads to precise values of the three principal birefringences and the optical orientation. The method is also able to obtain information on preferred orientation in a biaxial polycrystalline material, providing comprehensive information on both optical orientation of crystallites and spatial resolution. In addition, an unknown crystalline material may be identified, or at least classified within a specific group of crystalline materials.

 © 2006 International Union of Crystallography  
 Printed in Great Britain – all rights reserved

## 1. Introduction

In this paper, we apply a new optical technique for the three-dimensional examination of birefringent materials to optically biaxial crystals. The uniaxial case has already been considered in detail in a previous article (Pajdzik & Glazer, 2006).

In optically anisotropic crystals, light waves are transmitted with different velocities in different directions. Consider plane-polarized light passing through a biaxial crystal. In general, there are two different values of the phase velocity, defining two different refractive indices corresponding to a specified direction of propagation. These two values are associated with two mutually perpendicular polarizations, which means that the light is split into two light paths travelling subject to different refractive indices  $n''$  and  $n'$ . These refractive indices can be described by a cross section of a general ellipsoid known as the biaxial optical indicatrix, with semi-axes  $n_\alpha$ ,  $n_\beta$  and  $n_\gamma$ , where  $n_\alpha < n_\beta < n_\gamma$ . These are referred to as the principal refractive indices. This also introduces a phase difference between the two light paths with the result that when the two rays recombine, the final phase difference between them is a measure of the optical anisotropy of the sample corresponding to a specified propagation direction. The phase difference is given by

$$\delta = \frac{2\pi}{\lambda} (n'' - n')t, \quad (1)$$

where  $\lambda$  is the wavelength of the light,  $t$  is the thickness of the sample, and  $n'' - n'$  is the so-called plano-birefringence of the sample. Strictly speaking, the term birefringence, which is a characteristic of the sample, is obtained only when  $n''$  and  $n'$  coincide with  $n_\gamma$  and  $n_\alpha$ ,  $n_\gamma$  and  $n_\beta$ , or  $n_\beta$  and  $n_\alpha$ , respectively.

Measurement of optical linear birefringence has been one of the standard tools in the study of anisotropic properties of materials for nearly two centuries. Classically, birefringence is detected or measured using the crossed-polars technique and

compensators (see, for example, Hartshorne & Stuart, 1964, 1970). The classical technique is fast and easy; however, it suffers from a number of disadvantages. Firstly, if the birefringence of the sample is very low, it can be difficult to detect. Secondly, in this technique the sample must be oriented with respect to the polarization direction of the light and this makes the crossed-polars method impractical for determination of birefringence in non-homogenous samples, because the sample needs to be rotated to compare different regions simultaneously. Thirdly, classical compensation methods require manual point-by-point measurements. Finally, the accuracy of compensator measurements is limited. Because of this, some years ago we developed a new optical microscopy technique for automatically recording birefringence (Glazer *et al.*, 1996) which has subsequently been commercialized under the name Metripol (see <http://www.metripol.com>). This system uses a combination of a rotating polarizer and a circular analyser to separate out three types of images: one representing the light transmission  $I_0$  through the specimen, one showing the orientation angle  $\phi$  of one of the axes of a section of the optical indicatrix measured from the predetermined direction, and one giving quantitative information on  $|\sin \delta|$  at any point within the image captured by the CCD camera, where  $\delta$  is the phase difference introduced by the birefringent sample. The intensity of the light  $I$  measured at any position within the image captured by the CCD camera is a function of the angular orientation  $\alpha$  of the rotating polarizer and is defined by the following equation:

$$I = \frac{I_0}{2} [1 + \sin(2\phi - 2\alpha) \sin \delta]. \quad (2)$$

The Metripol technique has already been used for a broad range of applications (see, for example, Glazer *et al.*, 1996; Geday *et al.*, 2000; Shuvaeva *et al.*, 2005; Tixier *et al.*, 2005; Owen & Garman, 2005).

Recently, by adding a computer-controlled two-axis tilting stage, we have created a new version of the system, which is able to collect three-dimensional data in order to obtain precise birefringence information for optically anisotropic samples in any general orientation (Pajdzik & Glazer, 2006). A computer program was written in Visual C++ in order to perform the actual measurement process and the subsequent analysis of the data was carried out using *MATLAB* (<http://www.mathworks.com>). This program was designed to interface with the Metripol software. The current system fully reveals the three-dimensional character of the anisotropic properties of birefringent materials and thus provides a versatile optical technique, which may have applications in the fields of crystallography, mineralogy, geology, archaeology, chemistry, biology, *etc.* Furthermore, the method also makes possible automatic identification of an unknown crystalline material, or at least classification within a specific group of crystalline materials. However, one of the most important advantages of this technique is that for uniaxial and biaxial crystallites in polycrystalline materials, it provides comprehensive information on preferred orientation. Below we show how our method can obtain such texture information automatically for optically biaxial polycrystalline samples.

## 2. Tilting-stage technique

In §2.1 we present the derivation of the formulae. The equations derived here describe very well a mathematical model of the tilting-stage system for biaxial crystals in any general orientation. Subsequently, §2.2 illustrates an algorithm for the three-dimensional examination of optically biaxial crystals in order to obtain birefringence information, as well as to determine the optical orientation of biaxial samples. §2.3 presents the data analysis performed for a single crystal of a muscovite sheet with a thickness of 0.06 mm, while §2.4 shows the data analysis for a polycrystalline rock section of anhydrite with a thickness of 0.03 mm.

### 2.1. Derivation of formulae

Fig. 1 is a stereographic representation of the optical indicatrix for a biaxial sample.  $OA_1$  and  $OA_2$  represent the two optic axes which are separated by the optic angle  $2V$ . The  $x$ ,  $y$  and  $z$  axes correspond to the three principal refractive indices  $n_\beta$ ,  $n_\alpha$ , and  $n_\gamma$ , respectively. We assume here that the  $z$  axis is perpendicular to the plane of the drawing.  $S$  represents the general direction of propagation of the light within the biaxial sample (wave-normal direction), for which the value of  $|\sin \delta|$  is being measured. The direction  $S$  makes angles  $\vartheta_1$  and  $\vartheta_2$  with the optic axes  $OA_1$  and  $OA_2$ , respectively. OAP denotes the optic axial plane containing the two optic axes.

Taking into consideration the relations defining the two possible phase velocities  $v'_p$  and  $v''_p$  for a given direction of propagation  $S$  within the biaxial sample (see Appendix A; symbol definitions are listed in Appendix B),

$$v'_p{}^2 = \frac{1}{2}[v_\alpha^2 + v_\gamma^2 + (v_\alpha^2 - v_\gamma^2) \cos(\vartheta_1 - \vartheta_2)] \quad (3)$$

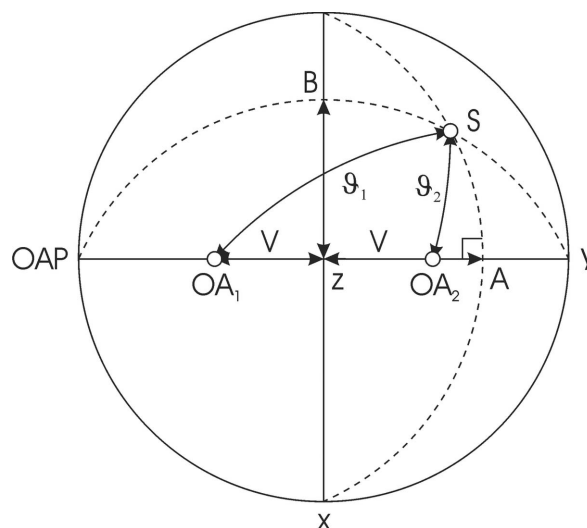


**Figure 1**  
Stereographic representation of the optical indicatrix for a biaxial sample.

and

$$v''_p{}^2 = \frac{1}{2}[v_\alpha^2 + v_\gamma^2 + (v_\alpha^2 - v_\gamma^2) \cos(\vartheta_1 + \vartheta_2)], \quad (4)$$

we can obtain the following expression:

$$v'_p{}^2 - v''_p{}^2 = (v_\alpha^2 - v_\gamma^2) \sin \vartheta_1 \sin \vartheta_2. \quad (5)$$

Using refractive indices instead of velocities, equation (5) becomes

$$\frac{1}{n'^2} - \frac{1}{n''^2} = \left( \frac{1}{n_\alpha^2} - \frac{1}{n_\gamma^2} \right) \sin \vartheta_1 \sin \vartheta_2. \quad (6)$$

Since the birefringence  $\Delta n_{\gamma\alpha} = n_\gamma - n_\alpha$  usually takes a small value, we can write to a good approximation<sup>1</sup> the value of the birefringence  $\Delta n_S$  (in general the plano-birefringence) measured down the propagation direction  $S$  in the following form (see, for example, Ramachandran & Ramaseshan, 1961):

$$\Delta n_S \simeq (n_\gamma - n_\alpha) \sin \vartheta_1 \sin \vartheta_2. \quad (7)$$

Note that, although  $n_\beta$  does not appear in equations (6) and (7) explicitly, it is involved implicitly in the definition of the relationships for the angles  $\vartheta_1$  and  $\vartheta_2$ .

Using spherical trigonometry with Fig. 1 and denoting the angles  $z$ - $A$  and  $z$ - $B$  as  $\psi_1$  and  $\psi_2$ , respectively, we obtain

$$\cos \vartheta_1 = \cos(V + \psi_1) \cos \psi_2 \quad (8)$$

and

$$\cos \vartheta_2 = \cos(V - \psi_1) \cos \psi_2. \quad (9)$$

$\psi_1$  is the component angle of  $S$  measured from the  $z$  axis projected onto the optic axial plane OAP, and  $\psi_2$  is the corresponding component angle of  $S$  projected on the  $xz$  plane perpendicular to OAP.

Taking into account equations (8) and (9), equation (7) becomes

<sup>1</sup> The difference between refractive indices is usually much smaller than their values.

$$\Delta n_S \simeq \Delta n_{\gamma\alpha} [1 - \cos^2(V + \psi_1) \cos^2 \psi_2]^{1/2} \times [1 - \cos^2(V - \psi_1) \cos^2 \psi_2]^{1/2}. \quad (10)$$

Using the Metripol technique, we actually measure  $|\sin \delta|$  and therefore we can write

$$|\sin \delta_S| \simeq \left| \sin \left( \frac{2\pi t}{\lambda} \Delta n_{\gamma\alpha} \right) \right|, \quad (11)$$

where  $|\sin \delta_S|$  denotes the value of  $|\sin \delta|$  measured down the direction of propagation  $S$  within the biaxial sample. Thus equation (10) becomes

$$|\sin \delta_S| \simeq \left| \sin \left\{ \frac{2\pi t}{\lambda} \Delta n_{\gamma\alpha} [1 - \cos^2(V + \psi_1) \cos^2 \psi_2]^{1/2} \times [1 - \cos^2(V - \psi_1) \cos^2 \psi_2]^{1/2} \right\} \right|. \quad (12)$$

Fig. 2 is a stereographic representation of the optical indicatrix for two different positions of the microscope tilting stage,  $S'$  and  $S$ . Assuming that the position  $S'$  corresponds to the direction of propagation of the light normal to the sample plane, *i.e.* before tilting, and the position  $S$  denotes the direction of propagation after tilting, we can decompose angles  $\psi_1$  and  $\psi_2$  into two components in the following way:

$$\psi_1 = \theta_1 + \omega_1 \quad (13)$$

and

$$\psi_2 = \theta_2 + \omega_2. \quad (14)$$

Thus equation (12) becomes

$$|\sin \delta_S| \simeq \left| \sin \left\{ \frac{2\pi t}{\lambda} \Delta n_{\gamma\alpha} \times [1 - \cos^2(V + \theta_1 + \omega_1) \cos^2(\theta_2 + \omega_2)]^{1/2} \times [1 - \cos^2(V - \theta_1 - \omega_1) \cos^2(\theta_2 + \omega_2)]^{1/2} \right\} \right|. \quad (15)$$

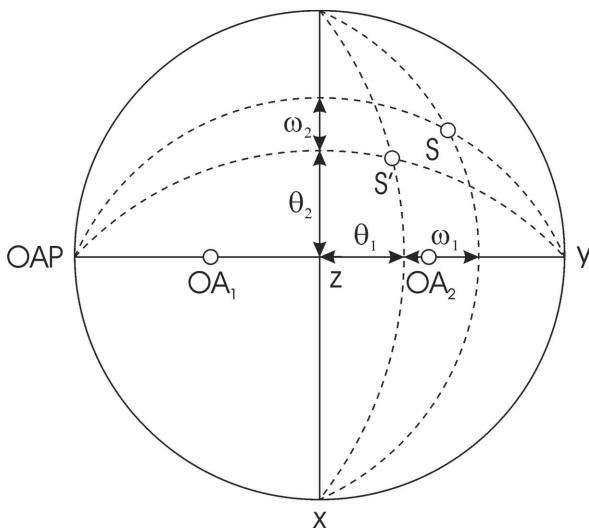


**Figure 2** Stereographic representation of the optical indicatrix for a biaxial sample for two different positions of the microscope tilting stage,  $S'$  and  $S$ .

In equation (15), angles  $\theta_1$  and  $\theta_2$  are the component angles of  $S'$  measured from the  $z$  axis projected on the optic axial plane OAP and the  $xz$  plane perpendicular to OAP, respectively. Angles  $\omega_1$  and  $\omega_2$  are internal tilt angles also measured along these planes.

Note that the two internal tilt angles  $\omega_1$  and  $\omega_2$  depend on the refractive indices of the sample and are different from the corresponding external tilt angles  $\Omega_1$  and  $\Omega_2$ , which are defined by the tilting of the microscope stage (Pajdzik & Glazer, 2006). In order to obtain the values of internal tilt angles, we can assume a mean refractive index of the biaxial sample and use Snell's law written in the following form:

$$\omega_1 \simeq \sin^{-1} \left( \frac{\sin \Omega_1}{n_{\text{mean}}} \right), \quad \omega_2 \simeq \sin^{-1} \left( \frac{\sin \Omega_2}{n_{\text{mean}}} \right). \quad (16)$$

In biaxial crystals, the mean refractive index of the sample can be calculated as (Wahlstrom, 1960)

$$n_{\text{mean}} = \frac{(n_\alpha + n_\beta + n_\gamma)}{3}. \quad (17)$$

For crystals with a large difference between the maximum and minimum refractive indices, the mean refractive index of the biaxial sample takes the following form (Wahlstrom, 1960):

$$n_{\text{mean}} = (n_\alpha n_\beta n_\gamma)^{1/3}. \quad (18)$$

Considering equations (16), equation (15) becomes

$$|\sin \delta_S| \simeq \left| \sin \left( \frac{2\pi t}{\lambda} \Delta n_{\gamma\alpha} \times \left\{ 1 - \cos^2 \left[ V + \theta_1 + \sin^{-1} \left( \frac{\sin \Omega_1}{n_{\text{mean}}} \right) \right] \times \cos^2 \left[ \theta_2 + \sin^{-1} \left( \frac{\sin \Omega_2}{n_{\text{mean}}} \right) \right] \right\}^{1/2} \times \left\{ 1 - \cos^2 \left[ V - \theta_1 - \sin^{-1} \left( \frac{\sin \Omega_1}{n_{\text{mean}}} \right) \right] \times \cos^2 \left[ \theta_2 + \sin^{-1} \left( \frac{\sin \Omega_2}{n_{\text{mean}}} \right) \right] \right\}^{1/2} \right) \right|. \quad (19)$$

Note that if the external tilt angles  $\Omega_1$  and  $\Omega_2$  are small, equation (19) can be written in a simplified form:

$$|\sin \delta_S| \simeq \left| \sin \left\{ \frac{2\pi t}{\lambda} \Delta n_{\gamma\alpha} \times \left[ 1 - \cos^2 \left( V + \theta_1 + \frac{\Omega_1}{n_{\text{mean}}} \right) \cos^2 \left( \theta_2 + \frac{\Omega_2}{n_{\text{mean}}} \right) \right]^{1/2} \times \left[ 1 - \cos^2 \left( V - \theta_1 - \frac{\Omega_1}{n_{\text{mean}}} \right) \cos^2 \left( \theta_2 + \frac{\Omega_2}{n_{\text{mean}}} \right) \right]^{1/2} \right\} \right|. \quad (20)$$

Furthermore, if the thickness of the sample  $t$  or the tilt angles are significant, then a thickness correction should be applied to the equations derived above (Pajdzik & Glazer, 2006). However, for most cases this correction is very small and can be neglected.

## 2.2. Data analysis

In the uniaxial case, in order to perform the analysis it is sufficient to find the principal section which contains the optic axis and the direction of propagation  $S'$  (Pajdzik & Glazer, 2006). For this principal section, one of the component angles of  $S'$  becomes equal to zero and the other is equal to the angle of the sample normal with respect to the optic axis. In order to locate this principal section, it is necessary first to find the value of the orientation angle  $\phi'$  corresponding to the direction of propagation  $S'$ , and subsequently to rotate the tilt axes  $\Theta_1$  and  $\Theta_2$  through the angle  $\phi'$ . In this way, the process of analysis is significantly simplified and the refinement of unknown parameters of the uniaxial sample such as the value of the birefringence  $\Delta n = n_e - n_o$ , the inclination angle  $\vartheta'$  measured between the optic axis and the direction of propagation  $S'$  and the mean refractive index  $n_{\text{mean}}$  are obtained by means of non-linear curve fitting applied to the data along this principal section.

The analysis of the three-dimensional data obtained from a biaxial sample is rather more difficult. In this case, the non-linear curve fitting has to be replaced by a more complicated surface fitting procedure. Note that for any general alignment of the biaxial sample, the two tilt axes  $\Theta_1$  and  $\Theta_2$  of the tilting stage will not necessarily be parallel to the optic axial plane OAP and the  $xz$  plane perpendicular to OAP, respectively. Furthermore, in order to carry out the analysis using equation (19), it is necessary to locate these directions.

In the uniaxial case, the orientation angle  $\phi$ , defined as the angle of one of the axes of a section of the optical indicatrix measured from the tilt axis  $\Theta_1$  of the tilting stage, for any position of the tilting stage indicates the principal section containing the optic axis and the specified direction of propagation. One of the axes of the relevant section of the optical indicatrix corresponds to the radial direction which coincides with this principal section, whereas the other corresponds to the tangential direction. Fig. 3 is a stereographic representation of the optical indicatrix showing the two permitted vibration directions corresponding to the direction of propagation  $S'$ . These vibration directions are determined using the Biot–Fresnel construction (see, for example, Bloss, 1961).

In the figure, the direction of propagation  $S'$  makes angles  $\vartheta'_1$  and  $\vartheta'_2$  with the optic axes  $OA_1$  and  $OA_2$ , respectively, and the dashed lines  $\Theta_1$  and  $\Theta_2$  represent traces of the two perpendicular tilt axes of the tilting stage. Note that in the biaxial case, the orientation angle  $\phi'$ , which is measured down the direction of propagation  $S'$ , in general, does not provide any information about the position of the plane parallel or perpendicular to OAP and containing the direction of propagation  $S'$  because the two axes of a section of the optical indicatrix usually do not coincide with these planes. The orientation angle  $\phi$  is the angle of one of the axes of a section of the optical indicatrix measured from the tilt axis  $\Theta_1$  of the tilting stage, and each time  $|\sin \delta|$  passes through zero, the computed value  $\phi$  changes through  $90^\circ$ . This ambiguity results from the fact that  $m\pi$ , where  $m$  is a positive integer, can be added to the measured relative phase difference  $\delta_0$  for positive

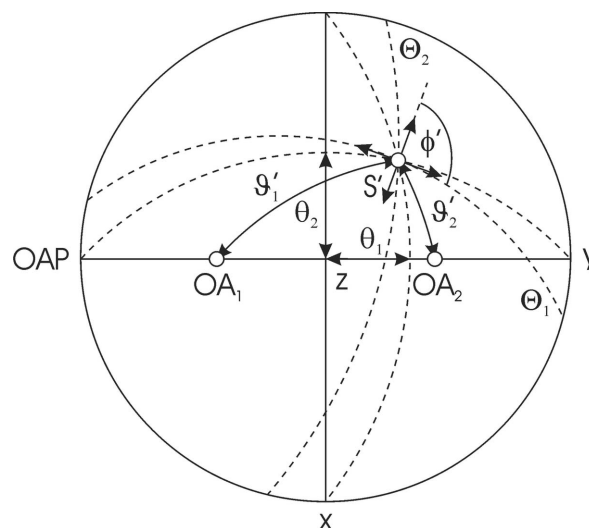


**Figure 3**

Stereographic representation of the optical indicatrix for a biaxial sample representing the two permitted vibration directions corresponding to the direction of propagation  $S'$  and determined using the Biot–Fresnel construction. The dashed lines marked  $\Theta_1$  and  $\Theta_2$  are traces of the two perpendicular tilt axes of the tilting stage. The orientation angle  $\phi'$  corresponds to the direction of propagation  $S'$  and represents the angle between the tilt axis  $\Theta_1$  and one of the axes of the relevant section of the optical indicatrix.

slopes of the  $|\sin \delta|$  function, or to  $-\delta_0$  for negative slopes of the  $|\sin \delta|$  function without change of  $|\sin \delta|$  itself. This means that

$$|\delta| = \delta_0 + m\pi \quad \text{or} \quad |\delta| = -\delta_0 + m\pi \quad (21)$$

for positive and negative slopes of  $|\sin \delta|$ , respectively, and

$$\delta_0 = \sin^{-1}(|\sin \delta|). \quad (22)$$

For  $m = 0$ , for which the ambiguity does not appear, the orientation angle  $\phi$  corresponds to the slow axis of the specified section of the optical indicatrix.

In the biaxial case, in order to find the positions of the planes parallel and perpendicular to OAP and containing the direction of propagation  $S'$ , we rotate the tilt axes of the  $|\sin \delta|$  contour map through a small angle  $\Delta\sigma$  and subsequently we apply a surface fitting procedure to the whole set of data using equation (19).<sup>2</sup> The rotation operation is then repeated and the surface fitting procedure is applied again. By repeating these steps over the angular range of  $0 \leq \sigma < 180^\circ$  and by analysing the corresponding fitting errors and the values of the refined parameters, it is possible to find the best fitted directions parallel and perpendicular to the optic axial plane OAP containing the direction of propagation  $S'$  and thus to obtain the orientation information of the biaxial sample. Note that because of symmetry, for  $180 \leq \sigma < 360^\circ$ , we obtain the same absolute values of the refined parameters as within the angular range  $0 \leq \sigma < 180^\circ$ . The difference is only in the signs of the component angles  $\theta_1$  and  $\theta_2$ . This introduces an ambiguity in determining the correct component angles  $\theta_1$  and  $\theta_2$ , for

<sup>2</sup> Note that the rotation of the tilt axes of the  $|\sin \delta|$  contour map through an angle  $\Delta\sigma$  is equivalent to the rotation of the  $|\sin \delta|$  contour map through an angle  $-\Delta\sigma$ .

example in preferred orientation studies where the sign of the component angles matters. However, for most cases this can be easily solved by analysing the shape of the corresponding  $|\sin \delta|$  contour map (see §2.4).

In equation (19), the angle  $V$ , the corresponding component angles  $\theta_1$  and  $\theta_2$ , and the mean refractive index  $n_{\text{mean}}$  are highly correlated. This means that in order to perform the analysis, additional knowledge of approximate values of at least one or preferably two parameters of the sample is required. Substituting the initial values for the angle  $V$  and the mean refractive index  $n_{\text{mean}}$  into equation (19) helps to refine precise values of the birefringence  $\Delta n_{\gamma\alpha}$  and the component angles  $\theta_1$  and  $\theta_2$ . Furthermore, after these operations, it is possible to adjust the initial values for  $V$  and  $n_{\text{mean}}$  by means of minimizing the fitting error and thus to find an even better solution.

The algorithm presented below is summarized by the following sequence of steps.

Step 1. Collect data on the Metrpol system for a large set of tilt angles of the biaxial sample within a specified range of the two perpendicular tilt axes  $\Theta_1$  and  $\Theta_2$  of the tilting stage.

Step 2. Assume initial values of the optic angle  $2V$  and preferably also of the mean refractive index  $n_{\text{mean}}$  of the biaxial sample.

Step 3. Apply surface fitting to the whole set of data using equation (19) and record values of the corresponding fitting error and the estimated parameters.

Step 4. Rotate the tilt axes of the  $|\sin \delta|$  contour map through a small angle  $\Delta\sigma$ .

Step 5. Repeat steps 3 and 4 over the angular range of  $0 \leq \sigma < 180^\circ$  and record the corresponding fitting errors and the estimated parameters.

Step 6. By analysing the fitting errors, the refined parameters and the shape of the corresponding  $|\sin \delta|$  contour map, among all the solutions, choose the one corresponding to the most probable values of the birefringence  $\Delta n_{\gamma\alpha}$  and the component angles  $\theta_1$  and  $\theta_2$  and hence the most probable directions of the planes which are parallel and perpendicular to the optic axial plane OAP and contain the direction of propagation  $S'$ .

Step 7. For the chosen solution, adjust the initial values of the angle  $V$  and the mean refractive index  $n_{\text{mean}}$  of the biaxial sample and subsequently reapply the surface fitting procedure in order to minimize the fitting error and thus find an even better solution.

Applying the algorithm to the measured  $|\sin \delta|$  data sometimes gives several solutions with high  $R^2$  values.<sup>3</sup> In this case, there is a need to use an additional criterion which would allow one to choose the correct result. Some of the proposed solutions can be easily ignored if the refined values of the birefringence  $\Delta n_{\gamma\alpha}$  (or the mean refractive index  $n_{\text{mean}}$ ) of the

<sup>3</sup> In order to measure the goodness of fit, we usually use several different statistics. However, in this paper we present results only for one of them, *i.e.* the  $R^2$  statistic. The coefficient is defined as the ratio of the sum of squares due to regression (SSR) and the total sum of squares (SST). The term 'sum of squares' means the sum of squared differences between predicted values and the mean (SSR) or between measured values and the mean (SST).

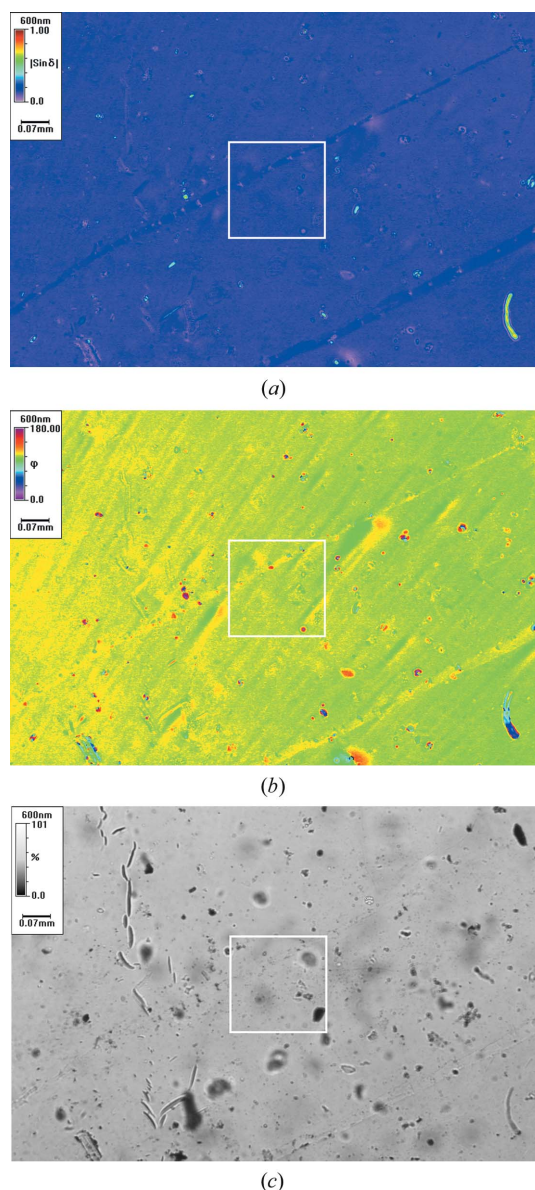


**Figure 4** Sample images of (a)  $|\sin \delta|$ , (b) orientation angle  $\phi$  and (c) light transmission  $I_0$  measured for a muscovite sheet with a thickness of 0.06 mm. The images correspond to the external tilt angles  $\Theta_1$  and  $\Theta_2$  of the tilting stage set equal to zero.

sample lie outside a range given by the literature. Otherwise, when this criterion cannot be applied, in order to choose the correct solution, we use the information on the orientation angle  $\phi'$  measured down the direction of propagation  $S'$ .

For each possible solution we can easily determine the two permitted vibration directions corresponding to the direction of propagation  $S'$  using the Biot–Fresnel construction (see Fig. 3). Having done this, it is possible to locate the positions of the two tilt axes  $\Theta_1$  and  $\Theta_2$  of the tilting stage using information on the orientation angle  $\phi'$ .

As mentioned before, the orientation angle  $\phi'$  represents the angle of one of the axes of a section of the optical indicatrix measured anticlockwise from the tilt axis  $\Theta_1$  of the tilting stage. For each proposed solution, by using the refined

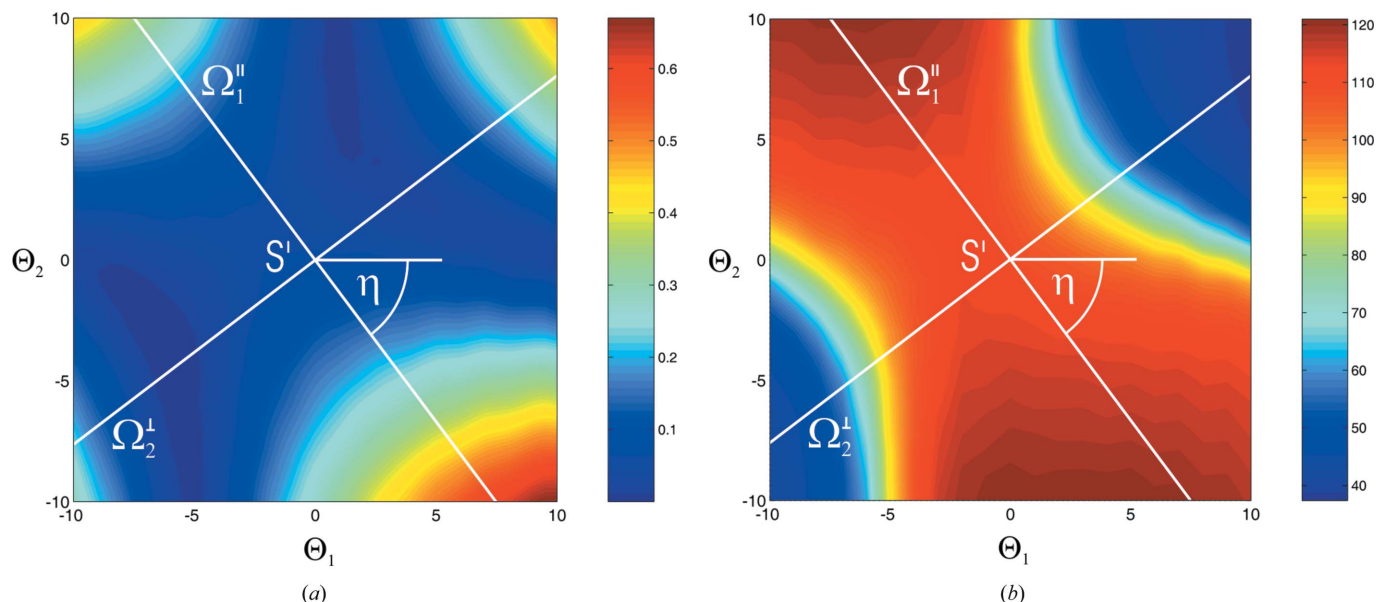


**Figure 5**  
 (a)  $|\sin \delta|$  and (b)  $\phi$  as a function of the two external tilt angles  $\Theta_1$  and  $\Theta_2$  for a muscovite sample with a thickness of 0.06 mm. The measurement was carried out at a wavelength of 600 nm for a total of 441 positions of the tilting stage.

parameters and taking into account the ambiguity expressed by equations (21) and (22) and also the ambiguity in the computed value of  $\phi'$ , we can easily determine for the specified slope of the  $|\sin \delta|$  function to which axis of the relevant section of the optical indicatrix the orientation angle  $\phi'$  is being measured. Thus, the positions of the tilt axis  $\Theta_1$  and  $\Theta_2$  can be found unambiguously.

Note also that if the proposed solution is correct, the angular difference between the determined  $\Theta_1$  axis and the direction parallel to the optic axial plane OAP and containing the direction of propagation  $S'$  should be equal to the corresponding angle  $\sigma$  for which the highest  $R^2$  value is found using the sequence of steps given above.

### 2.3. Three-dimensional birefringence information

As shown below, the tilting-stage technique applied to biaxial crystals allows us to obtain three-dimensional birefringence information as well as to determine the optical orientation of biaxial samples. Below we present results obtained for a single crystal of a muscovite sheet with a thickness of 0.06 mm. Muscovite is a common mineral which has a perfect basal cleavage yielding very thin laminae with (001) orientation.

Fig. 4 shows three types of images measured for a part of the muscovite sheet which correspond to the tilt angles of the tilting stage,  $\Theta_1$  and  $\Theta_2$  set equal to zero (propagation direction  $S'$ ). The first image provides quantitative information on  $|\sin \delta|$ ; the second illustrates the orientation angle  $\phi$  of one of the axes of the relevant section of the optical indicatrix measured from the horizontal direction within the image, and the third gives information on the light transmittance  $I_0$  through the sample. The rectangle shown in the figures

represents the set of pixels for which average values of  $|\sin \delta|$  and the orientation angle  $\phi$  were subsequently calculated.

Fig. 5 is a graphical representation of  $|\sin \delta|$  and  $\phi$  as a function of the two tilt angles  $\Theta_1$  and  $\Theta_2$  collected for the muscovite sample. As in the uniaxial case (Pajdzik & Glazer, 2006), the 441 data points were calculated as average values taken only from a small portion of the actual collected images (see rectangle marked in Fig. 4).

Fig. 5 shows that the contours form hyperbolic curves characteristic of the (001) orientation of the muscovite sheet. From the properties of the biaxial optical indicatrix, it is known that for directions of propagation which coincide with the optic axial plane OAP, one of the axes of a section of the optical indicatrix lies within OAP and the other is perpendicular to it (see, for example, Bloss, 1961). A similar situation can be observed for the  $xz$  plane perpendicular to OAP. In this case, one of the axes of a section of the optical indicatrix lies within this plane and the other is parallel to OAP. This also means that here, for this particular orientation of the muscovite sample, the orientation angle  $\phi$  provides information about the location of these two planes. Thus, by analysing the information on the orientation angle  $\phi$  given by Fig. 5(b), it is possible to find approximately<sup>4</sup> the two probable locations of the optic axial plane OAP. Note also that by taking into consideration only Fig. 5(b), it is difficult to judge which direction corresponds to the optic axial plane OAP and which corresponds to the plane  $xz$  perpendicular to OAP because of the 90° ambiguity introduced in the computed value of  $\phi$ .

<sup>4</sup> The propagation direction  $S'$  does not coincide exactly with the specified axis of the optical indicatrix because muscovite belongs to the monoclinic crystal system. There is also a small shift in the perpendicular direction, possibly because of a very small error in positioning the tilting stage with respect to the axis of the optical system.

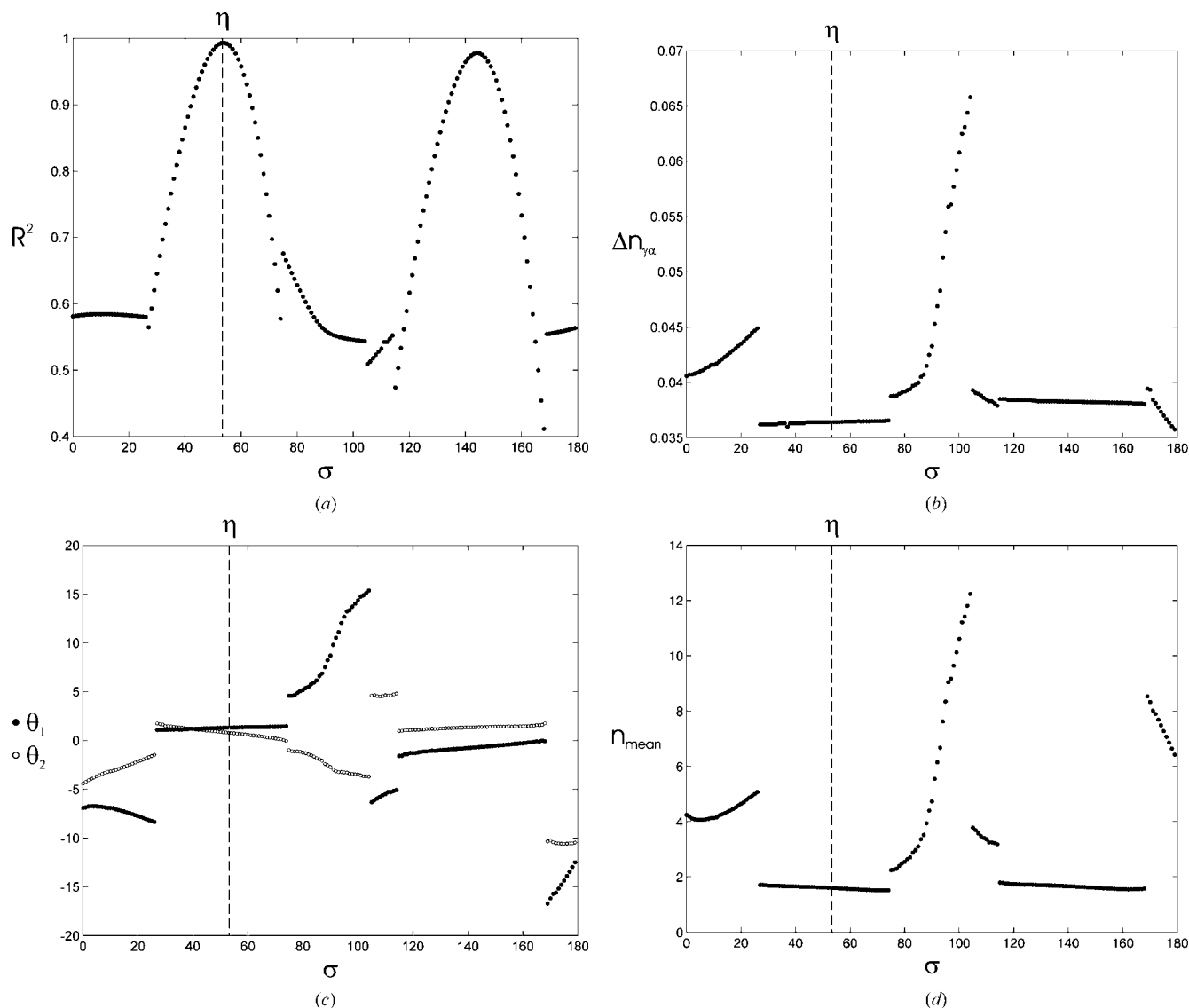


**Figure 6** (a)  $R^2$  and the refined values of the (b) birefringence  $\Delta n_{\gamma\alpha}$ , (c) component angles  $\theta_1$  and  $\theta_2$ , and (d) mean refractive index  $n_{\text{mean}}$  corresponding to different angular positions  $\sigma$  of the tilt axes.

Below, in order to obtain the value of the birefringence  $\Delta n_{\gamma\alpha}$  as well as to determine the optical orientation of the muscovite sample with respect to one of the principal axes of the optical indicatrix,<sup>5</sup> we carry out the analysis of the three-dimensional data by applying the steps given in §2.2. Since the optical sign of muscovite is negative, we assume that the  $z$  axis from Fig. 1 corresponds here to the refractive index  $n_\alpha$ , and the optic angle denoted as  $2V_\alpha$  is measured through this axis. Furthermore, because of the high correlation between the angle  $V_\alpha$  and the corresponding component angle  $\theta_1$ , we substitute into equation (19) a value of  $V_\alpha$  equal to  $21.5^\circ$ , which corresponds to the  $V_\alpha$  angle range given by the litera-

ture. The value of the angle  $V_\alpha = 21.5^\circ$  was chosen after performing a rough surface fitting procedure applied to the data for different angular positions of the tilt axes of the  $|\sin \delta|$  contour map for different initial values of  $V_\alpha$ , and after observing the behaviour of the estimated parameters and the fitting errors.

Subsequently, by rotating the tilt axes of the  $|\sin \delta|$  contour map over the angular range of  $180^\circ$  in steps of  $\Delta\sigma = 1^\circ$ , applying the surface fitting procedure to the data using equation (19) and then by analysing the corresponding fitting errors and the estimated parameters  $\Delta n_{\gamma\alpha}$ ,  $\theta_1$ ,  $\theta_2$  and  $n_{\text{mean}}$ , we can determine the directions parallel and perpendicular to the optic axial plane OAP containing the direction of propagation  $S'$ . These directions are marked in Fig. 5 by thick white lines labelled  $\Omega_1^\parallel$  and  $\Omega_2^\perp$ .

Fig. 6(a) shows  $R^2$  values for different angular positions  $\sigma$  of the tilt axes of the  $|\sin \delta|$  contour map. In the region where

<sup>5</sup> Using this technique we determine the orientation of the biaxial sample with respect to one of the axes of the optical indicatrix, which, in general, does not have to coincide with any of the crystallographic axes of the biaxial sample, as in monoclinic and triclinic crystal systems (see, for example, Born & Wolf, 1999; Wahlstrom, 1960).

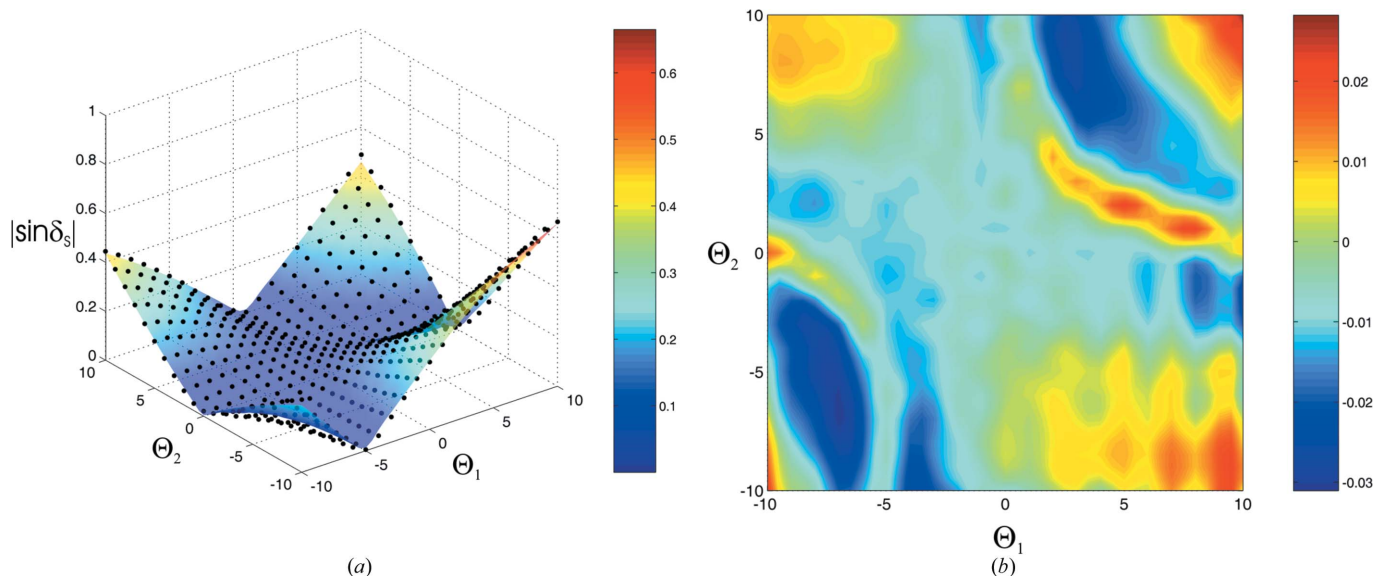


**Figure 7**  
 (a) Surface fitting applied to the measured  $|\sin \delta|$  data for the angular position of the tilt axes  $\sigma = 53.5^\circ$  and (b) corresponding residual plot.

$R^2 \rightarrow 1$ , we used smaller angular steps of  $\Delta\sigma = 0.5^\circ$  in order to determine the specified directions more precisely. By analysing the results, we found that  $R^2$  reaches its maximum, equal to 0.9935, for an angle  $\sigma = 53.5^\circ$ , measured clockwise from the tilt axis  $\Theta_1$  in Fig. 6. In the figure, this angle is denoted by  $\eta$ . By analysing the results presented in Fig. 6(a), we also found that a good surface fitting was recorded for an angle  $\sigma = 143.5^\circ$  with  $R^2 = 0.9777$  (exactly  $90^\circ$  difference from the  $53.5^\circ$  position of the rotated tilt axes). However, this latter result can be discarded by choosing the case with larger  $R^2$ . Moreover, for  $\sigma = 143.5^\circ$ , the refined value of  $n_{\text{mean}}$  lies slightly outside the literature range of the refractive indices for the muscovite sample (also for different initial values of  $V_\alpha$ ). A simple measurement of the optical retardation with a first-order retardation plate and a Michel–Lévy chart confirmed that the angular position  $\sigma = 53.5^\circ$  corresponds to the plane parallel to the optic axial plane OAP (see, for example, Wahlstrom, 1960).

Fig. 6(b) shows the refined values of the birefringence  $\Delta n_{\gamma\alpha}$ , Fig. 6(c) gives the refined values of the component angles  $\theta_1$  and  $\theta_2$  and Fig. 6(d) presents the refined values of the mean refractive index  $n_{\text{mean}}$  corresponding to different angular positions  $\sigma$ . The value of  $\Delta n_{\gamma\alpha}$  which corresponds to the best fit was recorded as  $0.036 \pm 0.001$ , the component angles  $\theta_1$  and  $\theta_2$  were found to be equal to  $1.3 \pm 0.5^\circ$  and  $0.8 \pm 0.5^\circ$ , and the mean refractive index  $n_{\text{mean}}$  was equal to  $1.60 \pm 0.05$ , respectively. Note also that the best surface fitting corresponds well with the literature range of the birefringence  $\Delta n_{\gamma\alpha}$ , 0.036–0.049 (see, for example, Deer *et al.*, 1992).

Finally, after these operations it is possible to adjust the initial value for  $V_\alpha$  by means of minimizing the fitting error and thus to find an even better solution. In order to realize this, the initial value for  $V_\alpha$  was changed in a specified range in steps of  $0.5^\circ$  followed by the surface fitting procedure. At the same time, the corresponding fitting error was observed. This process was carried out also for different angular positions of

the tilt axis close to the value  $\eta$ . Eventually, minimizing the fitting error by adjusting the initial value for  $V_\alpha$ , followed by the surface fitting procedure, did not change significantly the refined values of the birefringence  $\Delta n_{\gamma\alpha}$  and the component angles  $\theta_1$  and  $\theta_2$ . The mean refractive index  $n_{\text{mean}}$  was found to be equal to  $1.58 \pm 0.05$  and the adjusted value of  $V_\alpha$  for which the best result was recorded was equal to  $22 \pm 0.5^\circ$ . Furthermore, adjustments of the assumed angle  $V_\alpha$  did not change the position of the tilt axes for which  $R^2$  reached its maximum.

Fig. 7(a) illustrates the surface fitting applied to the measured data (marked by black points) using equation (19) for the angular position of the tilt axes  $\sigma = 53.5^\circ$ . Fig. 7(b) also shows the corresponding residual plot. In the figure, we can see that the residual plot shows systematic differences, presumably caused by the approximations used in the equations. However, the residuals are very small.

Note that the value of the birefringence measured for the direction of propagation corresponding to the  $n_\alpha$  axis is equal to  $\Delta n_{\gamma\beta} = n_\gamma - n_\beta$ . For this direction, the component angles  $\psi_1$  and  $\psi_2$  are equal to  $0^\circ$ . Similarly, for the direction of propagation corresponding to the  $n_\gamma$  axis, the birefringence is equal to  $\Delta n_{\beta\alpha} = n_\beta - n_\alpha$ . In this case, the component angle  $\psi_1 = 90^\circ$  and the component angle  $\psi_2 = 0^\circ$ . Thus, by using the refined value of the birefringence  $\Delta n_{\gamma\alpha}$  and the adjusted angle  $V_\alpha$ , we can calculate the other two principal birefringences, *i.e.*  $\Delta n_{\gamma\beta}$  and  $\Delta n_{\beta\alpha}$ , using the special cases of equation (10) written in the following forms:

$$\Delta n_{\gamma\beta} \simeq \Delta n_{\gamma\alpha} \sin^2 V \tag{23}$$

and

$$\begin{aligned} \Delta n_{\beta\alpha} &\simeq \Delta n_{\gamma\alpha} [1 - \cos^2(V + 90^\circ)]^{1/2} [1 - \cos^2(V - 90^\circ)]^{1/2} \\ &= \Delta n_{\gamma\alpha} \cos^2 V. \end{aligned} \tag{24}$$

By evaluating equations (23) and (24), we obtain the values of  $\Delta n_{\gamma\beta} = 0.005 \pm 0.001$  and  $\Delta n_{\beta\alpha} = 0.031 \pm 0.001$ , which

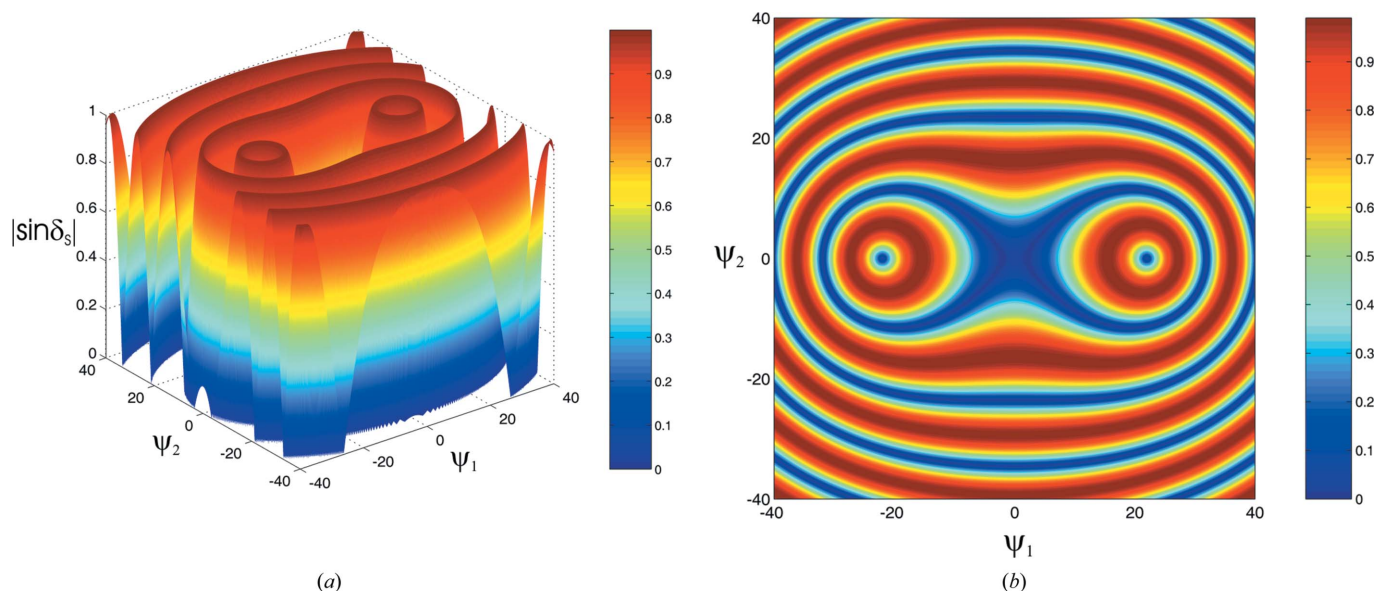


**Figure 8**  
 (a) Three-dimensional representation of  $|\sin \delta|$  with (b) two-dimensional contour map as a function of the two internal angles  $\psi_1$  and  $\psi_2$ .

correspond well with the literature values (see, for example, Deer *et al.*, 1992).

In order to check the results obtained using the tilting-stage technique, we estimated the value of the optic angle  $2V$  of the muscovite sample from a conoscopic figure. The estimated optic angle  $2V$  was found to be equal to  $45 \pm 2^\circ$ . Subsequently, we measured the value of the plano-birefringence corresponding to the 001 plane of the muscovite lamina using an Ehringhaus compensator. This value was found to be equal to  $0.0048 \pm 0.0002$ , which corresponds to the value of the principal birefringence  $\Delta n_{\gamma\beta} = 0.005 \pm 0.001$  obtained by means of the tilting-stage technique.

Taking into account the refined value of the birefringence  $\Delta n_{\gamma\alpha}$  and the adjusted angle  $V_\alpha$ , we can easily calculate the  $|\sin \delta|$  contour map for the muscovite sample using equation (12). Fig. 8 shows a three-dimensional representation of  $|\sin \delta|$  and a two-dimensional contour map as a function of the two internal angles  $\psi_1$  and  $\psi_2$ .<sup>6</sup> In order to simplify the calculations, the thickness of the sample was taken as a fixed value equal to 0.06 mm.

Note that here by applying the surface fitting to the whole set of data, we remove the ambiguity expressed by equations (21) and (22), because a large part of the three-dimensional shape of the  $|\sin \delta|$  function is very characteristic of the values of  $m$  [see equations (21) and (22)]. Therefore, in general, we are able to determine the component angles  $\theta_1$  and  $\theta_2$  and the birefringence  $\Delta n_{\gamma\alpha}$  directly from the  $|\sin \delta|$  values. However, by considering equations (21), (22), (10) and the refined parameters, we can easily calculate the values of  $m$  as well as obtain the corresponding values of the phase difference  $\delta_s$ , optical retardance  $\Delta n_s t$  and plano-birefringence  $\Delta n_s$  for any position of the microscope tilting stage.

<sup>6</sup> Note that although the representation of the  $|\sin \delta|$  function in the Cartesian coordinate system requires equal spacing between angle units in the  $\psi_1$ - $\psi_2$  plane, it does not have any effect on the relations between variables and, moreover, makes the interpretation of the plot easier.

It is also worth pointing out here that this technique makes it possible to identify unknown biaxial single crystals or biaxial crystallites in rock sections. In order to achieve this, we can create a database containing the values of the birefringences  $\Delta n_{\gamma\alpha}$ , the optical angles  $2V$  measured through a specified axis of the optical indicatrix, and the mean refractive indices  $n_{\text{mean}}$  corresponding to specified biaxial samples. Subsequently, by substituting in the process of analysis the stored values of  $V$  with the corresponding mean refractive indices  $n_{\text{mean}}$ , and by observing the refined parameters with the relevant fitting error, this technique may identify an unknown biaxial sample or, at least, classify it within a specific group of biaxial samples.

#### 2.4. Preferred orientation of biaxial polycrystalline materials

Optical methods have many important advantages in preferred orientation studies. They not only provide information about the orientation of crystallites, but also about spatial resolution and shapes of grains within a sample. However, optical techniques for preferred orientation studies using a standard microscope universal stage are very complicated and time-consuming. Some optical techniques are also very difficult to automate and usually require the presence of an expert. On the other hand, some automated optical texture systems are fast but also limited to uniaxial crystals only or some groups of crystals (Heilbronner & Pauli, 1993; Heilbronner, 2000; Yun & Azuma, 1999). Moreover, in the biaxial case, optical techniques are often combined with other approaches such as X-ray diffraction in order to provide reliable orientation information.<sup>7</sup>

In the previous paper (Pajdzik & Glazer, 2006) we showed that our tilting-stage system provides an automated technique giving precise information on preferred orientation as well as on the birefringence of uniaxial crystallites. Below we show

<sup>7</sup> Comprehensive information on the preferred orientation techniques is given by Wenk & Van Houtte (2004) and Kocks *et al.* (1998).

how the system can provide similar information for a biaxial sample. This technique can easily detect any changes in anisotropy caused by strain and deformations formed during growth of the polycrystalline material. Furthermore, any changes occurring as a result of recrystallization or phase transformations can be precisely recorded and analysed. With the Metripol technique, each grain of the polycrystalline specimen can be analysed to very high precision. The highest possible resolution which can be achieved by the current optical system is equal to  $0.3\ \mu\text{m}$  with a  $50\times$  objective. This, combined with the possibility to identify unknown uniaxial and biaxial crystallites in a thin rock section, makes the tilting-stage technique an extremely useful and important tool in preferred orientation studies.

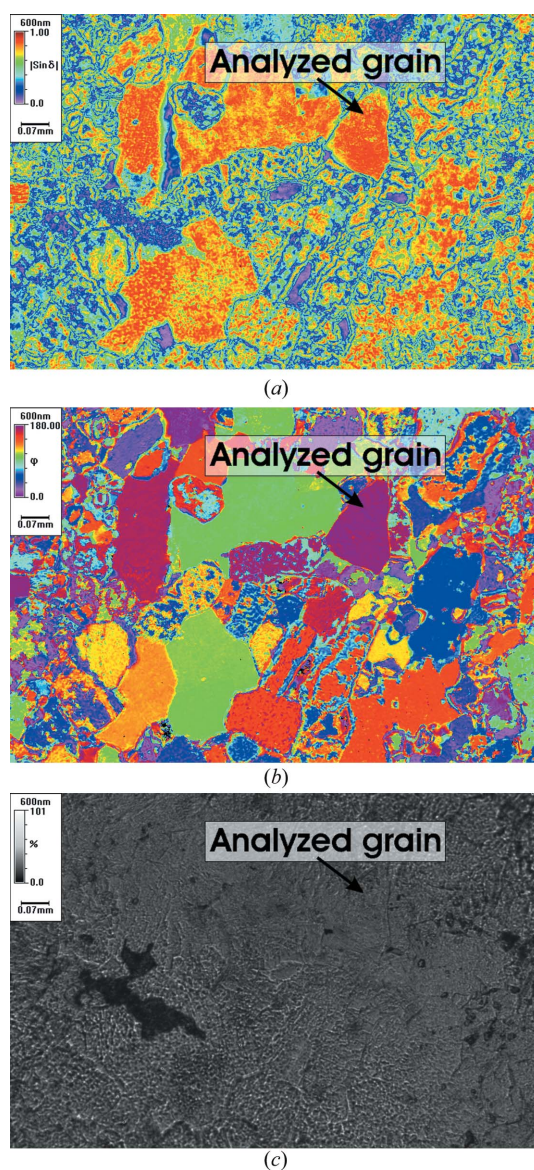
Fig. 9 shows  $|\sin \delta|$ , the orientation angle  $\phi$  and the light transmittance  $I_0$  images corresponding to tilt angles  $\Theta_1$  and  $\Theta_2$  of the tilting stage set equal to zero (propagation direction  $S'$ ) measured for a region of an anhydrite rock section from Yorkshire (UK) with a thickness of  $0.03\ \text{mm}$ .

Fig. 10 is a graphical representation of  $|\sin \delta|$  and  $\phi$  as a function of the two tilt angles  $\Theta_1$  and  $\Theta_2$ , collected for one single grain of the anhydrite rock section marked in Fig. 9. The measurement was carried out at a wavelength of  $600\ \text{nm}$  and a total of 441 data points were calculated as average values taken from a large part of the grain area. A complete set of measurements with the current setup took approximately 55 min. This usually provides three-dimensional data for many grains of a rock section (see, for example, Fig. 9). In Fig. 10(a), we can see that the contours form a portion of nearly concentric half circles characteristic of a position near one of the optic axes of the biaxial sample.

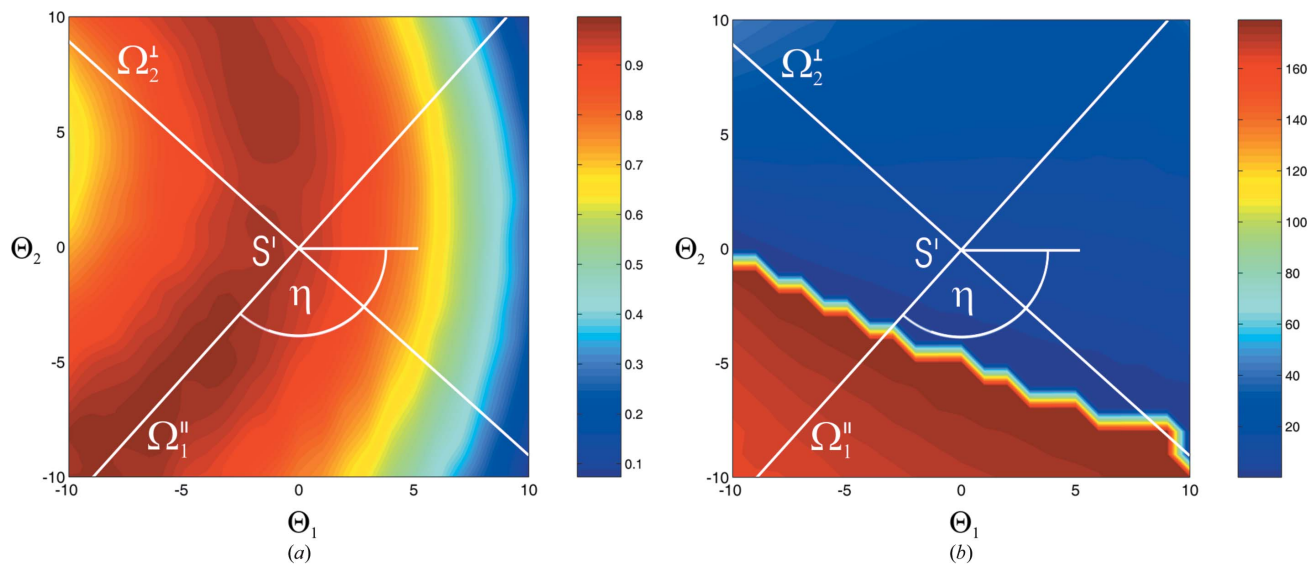
As with the analysis of the muscovite sample, we applied the algorithm given in §2.2. However, in this case, in order to obtain precise orientation information for all grains in the image, we assumed initial values of both the angle  $V$  and the mean refractive index  $n_{\text{mean}}$  of the sample. Assuming these two initial values improves the location of the correct residual minimum in the surface-fitting process and allows reliable comparison of orientation information between all the grains studied. Since the optical sign of anhydrite is positive, we assume that the  $z$  axis of Fig. 1 corresponds here to the refractive index  $n_\gamma$ , and the optic angle denoted as  $2V_\gamma$  is measured through this axis. The value of the angle  $V_\gamma$  was taken to be equal to  $21^\circ$ , which is within the  $V_\gamma$  angle range given in the literature, and a mean refractive index  $n_{\text{mean}}$  equal to  $1.584$  was calculated using equation (17) and the literature values for the principal refractive indices  $n_\gamma$ ,  $n_\beta$  and  $n_\alpha$  of the anhydrite sample.

Fig. 11(a) shows  $R^2$  for different angular positions  $\sigma$  of the tilt axes of the  $|\sin \delta|$  contour map. The highest  $R^2 = 0.9890$  was recorded only for  $\sigma = 132^\circ$ . Fig. 11(b) also shows the corresponding values of the birefringence  $\Delta n_{\gamma\alpha}$  and Fig. 11(c), the corresponding values of the component angles  $\theta_1$  and  $\theta_2$  refined for different angular positions  $\sigma$ . The value of the birefringence  $\Delta n_{\gamma\alpha}$  for which the best fit was recorded was equal to  $0.039$ . The values of component angles  $\theta_1$  and  $\theta_2$  were found to be  $-25.8^\circ$  and  $10.2^\circ$ , respectively.

Subsequently, minimizing the fitting error by adjusting the initial values for the angle  $V_\gamma$  and the mean refractive index  $n_{\text{mean}}$ , followed by the surface fitting procedure, allowed us to obtain even better values for the component angles  $\theta_1$  and  $\theta_2$ , equal to  $-26.8 \pm 0.5^\circ$  and  $9.9 \pm 0.5^\circ$ , respectively, and a value of the birefringence  $\Delta n_{\gamma\alpha}$  of  $0.039 \pm 0.001$ . This corresponds very well with the literature  $\Delta n_{\gamma\alpha}$  values of  $0.039\text{--}0.40$  (see, for example, Deer *et al.*, 1992). The values of the angle  $V_\gamma$  and the mean refractive index  $n_{\text{mean}}$  for which the best results were recorded were found to be  $22 \pm 0.5^\circ$  and  $1.60 \pm 0.05$ , respectively. In this way, the adjusted value of  $n_{\text{mean}}$  corresponds now to the mean value of the refractive indices for the specified set of the examined cross sections of the optical indicatrix rather than to the whole optical indicatrix.



**Figure 9** Sample images of (a)  $|\sin \delta|$ , (b) orientation angle  $\phi$  and (c) light transmittance  $I_0$  for a region of an anhydrite rock section with a thickness of  $0.03\ \text{mm}$ . The images correspond to the external tilt angles  $\Theta_1$  and  $\Theta_2$  of the tilting stage set equal to zero.



**Figure 10**  
 (a)  $|\sin \delta|$  and (b)  $\phi$  as a function of the two external tilt angles  $\Theta_1$  and  $\Theta_2$  for a single grain (marked in Fig. 9) of the anhydrite rock section with a thickness of 0.03 mm. The measurement was carried out at a wavelength of 600 nm for a total of 441 positions of the tilting stage. [The angular range of the orientation angle  $\phi$  measured by the Metripol system is  $0 \leq \phi \leq 180^\circ$ ; this causes the  $180^\circ$  step seen in Fig. 10(b).]

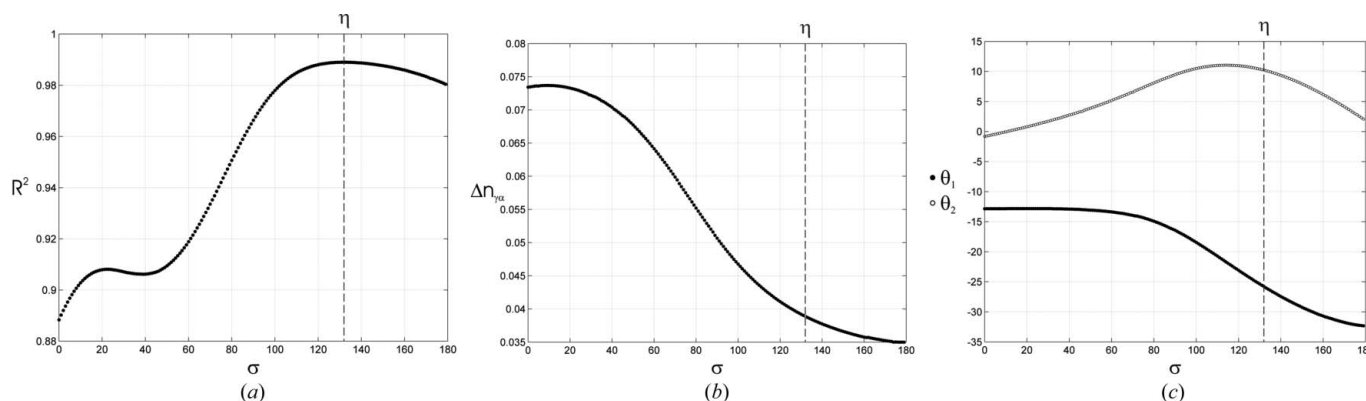


**Figure 11**  
 (a)  $R^2$  and the refined values of the (b) birefringence  $\Delta n_{\gamma\alpha}$  and (c) component angles  $\theta_1$  and  $\theta_2$  corresponding to different angular positions  $\sigma$  of the tilt axes.

Furthermore, adjusting the angle  $V_\gamma$  and the mean refractive index  $n_{\text{mean}}$  did not change the best estimated value of  $\sigma$ .

Fig. 12 shows surface fitting applied to the measured data (marked by black points) using equation (19) for  $\sigma = 132^\circ$ , along with the corresponding residual plot.

By using the refined value of the birefringence  $\Delta n_{\gamma\alpha}$  and the adjusted value of the angle  $V_\gamma$ , we can calculate the other two principal birefringences, *i.e.*  $\Delta n_{\gamma\beta}$  and  $\Delta n_{\beta\alpha}$  as presented in §2.3, obtaining the values of  $\Delta n_{\gamma\beta} = 0.034 \pm 0.001$  and  $\Delta n_{\beta\alpha} = 0.005 \pm 0.001$ .

As mentioned in §2.2, because of symmetry, for the rotation angles of the tilt axes within the angular range  $180 \leq \sigma < 360^\circ$ , we obtain the same absolute values of the refined parameters as within the angular range of  $0 \leq \sigma < 180^\circ$ . The difference is only in the signs of the component angles  $\theta_1$  and  $\theta_2$ . It is worth pointing out here that in preferred orientation studies in order to mark the component angles  $\theta_1$  and  $\theta_2$  on a stereographic plot, we have to solve this ambiguity. Fig. 13 shows the two possible solutions of the component angles: (1) in the angular

range  $0 \leq \sigma < 180^\circ$ , *i.e.*  $\theta_1 = -25.8 \pm 0.5^\circ$  and  $\theta_2 = 10.2 \pm 0.5^\circ$ , and (2) in the angular range  $180 \leq \sigma < 360^\circ$ , *i.e.*  $\theta_1 = 25.8 \pm 0.5^\circ$  and  $\theta_2 = -10.2 \pm 0.5^\circ$ , respectively marked by two white points. The corresponding  $|\sin \delta|$  contour map was calculated as a function of the two internal angles  $\psi_1$  and  $\psi_2$  using equation (12) for the refined value of the birefringence  $\Delta n_{\gamma\alpha}$  and the adjusted values of the angle  $V_\alpha$ . In order to simplify the calculations, the thickness of the sample was taken as a fixed value equal to 0.03 mm. Subsequently, by taking into account the curvature of the  $|\sin \delta|$  contour map shown in Fig. 10(a), we chose here solution (2) [the  $|\sin \delta|$  contour map shown in Fig. 10(a) rotated clockwise through an angle equal to  $180^\circ - \eta$  is consistent with the choice of solution (2)]. Note that this has an entirely conventional character and corresponds to the chosen alignment of the sample on the microscope stage.

Fig. 14 is a stereographic plot showing the orientation information for 21 different grains in the anhydrite rock section.

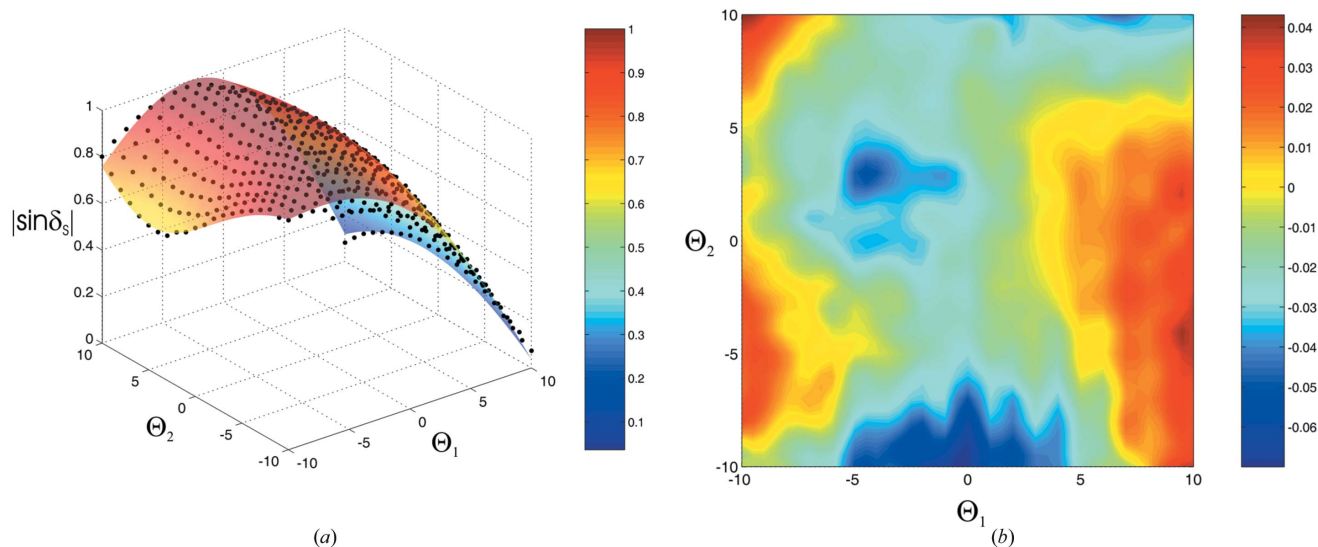


**Figure 12**  
(a) Surface fitting applied to the measured  $|\sin \delta|$  data for  $\sigma = 132^\circ$  and (b) corresponding residual plot.

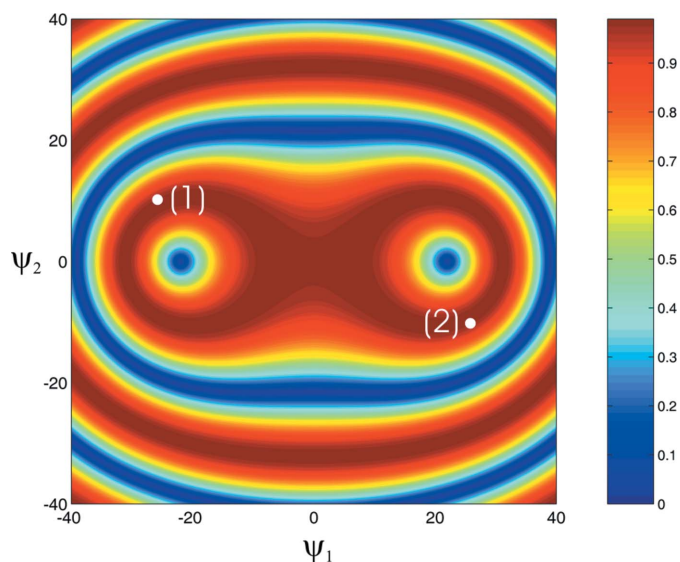


**Figure 13**  
Graph representing a  $|\sin \delta|$  contour map as a function of the two internal angles  $\psi_1$  and  $\psi_2$  showing the two possible solutions of the component angles  $\theta_1$  and  $\theta_2$  for the analysed grain (marked by two white points).

### 2.5. Precision of the technique

Equation (7) is based on the assumption that the difference between refractive indices is usually much smaller than their values. This equation is an approximation for which the error is small for samples with low and medium values of the birefringence. However, we have found that even for large birefringences, the results still seem reasonable.

The values of the estimated errors depend mainly on the value of the birefringence of the sample, the thickness of the sample and the precision with which the thickness is measured. Equation (16), used to obtain internal tilt angles, assumes the mean refractive index of the biaxial sample. This may be a source of error, which is comparatively larger for a sample with a high value of the birefringence. Furthermore, equation (20) assumes small angles. For tilt angles greater than

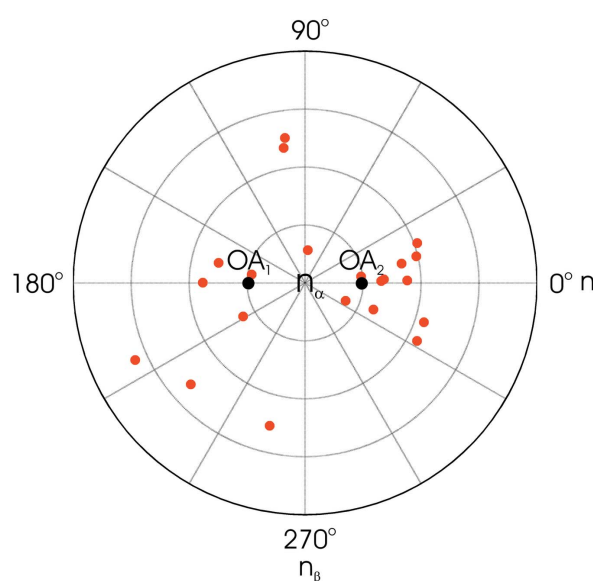


**Figure 14**  
Stereographic plot showing texture information in the anhydrite rock section (21 data points). The points denote the angles of the sample normal with respect to the indicatrix axes.

$10^\circ$ , this approximation gives an error which cannot be neglected and equation (19) should be used instead.

Finally, in estimating errors, one should take into consideration the thickness correction (Pajdzik & Glazer, 2006). If the thickness of the sample  $t$  or the tilt angles are significant, then a thickness correction should be applied to the equations derived in §2.1. In our technique, by setting the external tilt angles of the tilting stage typically from  $-10^\circ$  to  $10^\circ$ , for most of our samples we do not have to apply a thickness correction.

For the samples presented in this paper, we have estimated the corresponding errors by taking into account results obtained for different regions of the same sample and by consideration of the sources of errors discussed above. In estimating errors for the muscovite sample, we measured the

optic angle  $2V$  using a conventional conoscopic figure and the birefringence  $\Delta n_{\gamma\beta}$  with an Ehringhaus compensator (approximately because the [001] direction does not coincide precisely with the  $n_\alpha$  direction of the muscovite sample). As  $\Delta n_{\gamma\alpha}$  for the anhydrite section is similar, we can assume similar errors.

Note that the pleochroism can have an effect on measurements carried out using this apparatus. However, the technique uses monochromatic light and the choice of an appropriate filter may avoid the occurrence of the selective absorption for a specified direction of propagation within a crystal.

### 3. Conclusions

We have shown that by applying the tilting-stage technique to optically biaxial crystals, it is possible to collect three-dimensional data for  $|\sin \delta|$  and the orientation angle  $\phi$  in order to obtain precise three-dimensional birefringence information, as well as to determine the optical orientation of biaxial samples. The following information on biaxial samples can be obtained from the above technique.

- (i) Two-dimensional projections of lines of equal birefringence.
- (ii) The three principal birefringences  $\Delta n_{\gamma\alpha}$ ,  $\Delta n_{\gamma\beta}$  and  $\Delta n_{\beta\alpha}$ .
- (iii) The component angles  $\theta_1$  and  $\theta_2$  determining the optical orientation of the sample.
- (iv) The corresponding values of the phase difference  $\delta_s$ , and thus optical retardance  $\Delta n_s t$  and plano-birefringence  $\Delta n_s$ .
- (v) An estimate of the mean refractive index of the sample  $n_{\text{mean}}$ .
- (vi) Whether the sample is uniaxial or biaxial.
- (vii) Texture information from polycrystalline materials.
- (viii) Identification, or at least classification within a specific group of crystalline materials, of unknown samples.

### APPENDIX A

#### Phase velocities within the biaxial sample

Maxwell's equations for a nonmagnetic, homogeneous and transparent medium are defined by the following relations between the electric field  $\mathbf{E}$ , the electric displacement  $\mathbf{D}$ , the magnetic field  $\mathbf{H}$  and the magnetic induction  $\mathbf{B}$ :

$$\begin{aligned} -\mu_0 \frac{\partial \mathbf{H}}{\partial t} &= \nabla \times \mathbf{E}, \\ \frac{\partial \mathbf{D}}{\partial t} &= \nabla \times \mathbf{H}, \\ \nabla \cdot \mathbf{D} &= 0, \\ \nabla \cdot \mathbf{H} &= 0. \end{aligned} \tag{25}$$

For plane monochromatic waves given by

$$\mathbf{E} = \mathbf{E}_0 \exp[i(\mathbf{k} \cdot \mathbf{r} - \omega t)], \tag{26}$$

we obtain from Maxwell's equations:

$$\begin{aligned} \mu_0 i \omega \mathbf{H} &= i(\mathbf{k} \times \mathbf{E}), \\ -i \omega \mathbf{D} &= i(\mathbf{k} \times \mathbf{H}). \end{aligned} \tag{27}$$

In addition: (i) vector  $\mathbf{D}$  is perpendicular to the direction of the wavevector  $\mathbf{k}$  determining the propagation of the surface of constant phase; (ii) vectors  $\mathbf{D}$ ,  $\mathbf{E}$ ,  $\mathbf{k}$  and the Poynting vector  $\mathbf{S} = \mathbf{E} \times \mathbf{H}$  are coplanar; (iii) vectors  $\mathbf{S}$  and  $\mathbf{k}$  do not normally coincide in direction.

From equations (27) and

$$k^2 = \frac{\omega^2}{c^2} n^2, \quad \mathbf{k} = ks, \quad |s| = 1, \tag{28}$$

we obtain

$$\varepsilon_i E_i = n^2 [E_i - s_i (\mathbf{s} \cdot \mathbf{E})], \quad \text{where } i = 1, 2, 3. \tag{29}$$

This then leads to the result

$$\frac{s_1^2}{n^2 - \varepsilon_1} + \frac{s_2^2}{n^2 - \varepsilon_2} + \frac{s_3^2}{n^2 - \varepsilon_3} = \frac{1}{n^2}. \tag{30}$$

From equation (30) and

$$s_1^2 + s_2^2 + s_3^2 = 1, \quad v_i = \frac{c}{\varepsilon_i^{1/2}}, \quad v_p = \frac{c}{n}, \tag{31}$$

the Fresnel equation for the velocity of phase propagation of electromagnetic waves in an anisotropic medium (Born & Wolf, 1999) is obtained:

$$\frac{s_1^2}{v_p^2 - v_1^2} + \frac{s_2^2}{v_p^2 - v_2^2} + \frac{s_3^2}{v_p^2 - v_3^2} = 0. \tag{32}$$

For biaxial crystals, taking into account the Fresnel equation, we can write

$$\begin{aligned} s_1^2 (v_p^2 - v_\beta^2)(v_p^2 - v_\gamma^2) + s_2^2 (v_p^2 - v_\alpha^2)(v_p^2 - v_\gamma^2) \\ + s_3^2 (v_p^2 - v_\alpha^2)(v_p^2 - v_\beta^2) = 0. \end{aligned} \tag{33}$$

Using equations (31), equation (33) can be written as

$$\begin{aligned} v_p^4 - v_p^2 [s_1^2 (v_\beta^2 - v_\alpha^2) + s_3^2 (v_\beta^2 - v_\gamma^2) + v_\alpha^2 + v_\gamma^2] \\ + s_1^2 v_\gamma^2 (v_\beta^2 - v_\alpha^2) + s_3^2 v_\alpha^2 (v_\beta^2 - v_\gamma^2) + v_\alpha^2 v_\gamma^2 = 0. \end{aligned} \tag{34}$$

Assuming that the propagation vector  $\mathbf{s}$  makes angles  $\vartheta_1$  and  $\vartheta_2$  with the optic axes, and considering the following equalities,

$$\begin{aligned} s_1^2 &= \frac{1}{4} \frac{(v_\alpha^2 - v_\gamma^2)}{(v_\alpha^2 - v_\beta^2)} (\cos \vartheta_1 - \cos \vartheta_2)^2, \\ s_3^2 &= \frac{1}{4} \frac{(v_\alpha^2 - v_\gamma^2)}{(v_\beta^2 - v_\gamma^2)} (\cos \vartheta_1 + \cos \vartheta_2)^2, \end{aligned} \tag{35}$$

we can derive the solution given by (Petykiewicz, 1992)

$$v_p'^2 = \frac{1}{2} [v_\alpha^2 + v_\gamma^2 + (v_\alpha^2 - v_\gamma^2) \cos(\vartheta_1 - \vartheta_2)] \tag{36}$$

and

$$v_p''^2 = \frac{1}{2} [v_\alpha^2 + v_\gamma^2 + (v_\alpha^2 - v_\gamma^2) \cos(\vartheta_1 + \vartheta_2)]. \tag{37}$$

## APPENDIX B

### Notation

$\delta$ : phase difference.  
 $\lambda$ : wavelength of the light.  
 $n', n''$ : two possible refractive indices for a given direction of propagation of the light.  
 $n' - n''$ : effective birefringence projected onto the plane of the sample, the so-called plano-birefringence.  
 $t$ : thickness of the sample.  
 $I$ : intensity of the light measured at any position within the image captured by the CCD camera.  
 $I_0$ : intensity of unpolarized light transmitted through the sample.  
 $\phi$ : orientation angle of one of the axes of a section of the optical indicatrix measured from a predetermined direction.  
 $\alpha$ : angular orientation of the rotating polarizer.  
 $OA_1$  and  $OA_2$ : two optic axes of the biaxial sample.  
 $2V$ : optic angle of the biaxial sample.  
 $n_\gamma, n_\beta$  and  $n_\alpha$ : three principal refractive indices of the biaxial sample.  
 $S$ : general direction of propagation of the light within the sample (wave-normal direction).  
 OAP: optic axial plane.  
 $\vartheta_1$ : angle between the direction of propagation  $S$  and the optic axis  $OA_1$ .  
 $\vartheta_2$ : angle between the direction of propagation  $S$  and the optic axis  $OA_2$ .  
 $u'_p$  and  $u''_p$ : two possible phase velocities for a given propagation direction  $S$ .  
 $u_\gamma$ : phase velocity corresponding to the  $n_\gamma$  refractive index.  
 $u_\alpha$ : phase velocity corresponding to the  $n_\alpha$  refractive index.  
 $\Delta n_{\gamma\alpha}$ ,  $\Delta n_{\gamma\beta}$  and  $\Delta n_{\beta\alpha}$ : three principal birefringences of the biaxial sample, calculated as  $n_\gamma - n_\alpha$ ,  $n_\gamma - n_\beta$  and  $n_\beta - n_\alpha$ , respectively.  
 $\Delta n_S$ : plano-birefringence measured down the direction of propagation  $S$ .  
 $\delta_S$ : phase difference corresponding to the direction of propagation  $S$ .  
 $|\sin \delta_S|$ :  $|\sin \delta|$  measured down the direction of propagation  $S$ .  
 $\psi_1$ : component angle of  $S$  measured from the  $z$  axis projected on the optic axial plane OAP.  
 $\psi_2$ : component angle of  $S$  measured from the  $z$  axis projected on the  $xz$  plane perpendicular to OAP.  
 $S'$ : direction of propagation of the light normal to the sample, *i.e.* before tilting.  
 $\vartheta'_1$ : angle between the direction of propagation  $S'$  and the optic axis  $OA_1$ .  
 $\vartheta'_2$ : angle between the direction of propagation  $S'$  and the optic axis  $OA_2$ .  
 $\phi'$ : orientation angle  $\phi$  measured down the direction of propagation  $S'$ .  
 $\theta_1$ : component angle of  $S'$ , measured from the  $z$  axis, projected on the optic axial plane OAP.  
 $\theta_2$ : component angle of  $S'$ , measured from the  $z$  axis, projected on the  $xz$  plane perpendicular to OAP.

$\Theta_1$  and  $\Theta_2$ : two perpendicular external tilt angles of the tilting stage (also denote relative tilt axes).

$\Omega_1$ : external tilt angle measured along the optic axial plane OAP.

$\Omega_2$ : external tilt angle measured along the  $xz$  plane perpendicular to OAP.

$\omega_1$ : internal tilt angle measured along the optic axial plane OAP.

$\omega_2$ : internal tilt angle measured along the  $xz$  plane perpendicular to OAP.

$n_{\text{mean}}$ : mean refractive index.

$\delta_0$ : relative phase difference.

$m$ : positive integer.

$\sigma$ : angular position of the rotated tilt axes of the  $|\sin \delta|$  contour map.

$\Delta\sigma$ : a small angle (typically  $1^\circ$ ) defining an angular step.

$\Omega_1^\parallel$ : external tilt angle measured along the plane parallel to the optic axial plane OAP and containing the direction of propagation  $S'$ .

$\Omega_2^\perp$ : external tilt angle measured along the plane perpendicular to OAP which contains the direction of propagation  $S'$ .

$\eta$ : angular position of the rotated tilt axes of the  $|\sin \delta|$  contour map for which the highest  $R^2$  value is recorded.

**E**: electric field.

**D**: electric displacement.

**H**: magnetic field.

**B**: magnetic induction.

**k**: wavevector.

**S**: Poynting vector.

We are grateful to the Engineering and Physical Sciences Research Council for a grant that enabled this work to be carried out. We also would like to thank Dr Dave Waters, of the Earth Sciences Department at the University of Oxford, for the biaxial rock sections used in the preferred orientation study.

### References

- Bloss, F. D. (1961). *An Introduction to the Methods of Optical Crystallography*. New York: Holt, Rinehart and Winston.  
 Born, M. & Wolf, E. (1999). *Principles of Optics*. Cambridge University Press.  
 Deer, W. A., Howie, R. A. & Zussman, J. (1992). *The Rock-Forming Minerals*, 2nd ed. Harlow: Longman.  
 Geday, M. A., Kaminsky, W., Lewis, J. G. & Glazer, A. M. (2000). *J. Microsc.* **198**, 1–9.  
 Geday, M. A., Kreisel, J., Glazer, A. M. & Roleder, K. (2000). *J. Appl. Cryst.* **33**, 909–914.  
 Glazer, A. M., Lewis, J. G. & Kaminsky, W. (1996). *Proc. R. Soc. London Ser. A*, **452**, 2751–2765.  
 Hartshorne, N. H. & Stuart, A. (1964). *Practical Optical Crystallography*. London: Edward Arnold.  
 Hartshorne, N. H. & Stuart, A. (1970). *Crystals and the Polarizing Microscope*, 4th ed. London: Edward Arnold.  
 Heilbronner, R. P. (2000). *Optical Orientation Imaging*, in *Stress, Strain and Structure, a Volume in Honour of W. D. Means*, edited by M. W. Jessel & J. L. Urai. *J. Virtual Explorer*, **2**.  
 Heilbronner, R. P. & Pauli, C. (1993). *J. Struct. Geol.* **15**, 369–382.

- Kocks, U. F., Tome, C. N. & Wenk, H.-R. (1998). *Texture and Anisotropy. Preferred Orientations in Polycrystals and their Effect on Materials Properties*. Cambridge University Press.
- Owen, R. L. & Garman, E. (2005). *Acta Cryst.* **D61**, 130–140.
- Pajdzik, L. A. & Glazer, A. M. (2006). *J. Appl. Cryst.* **39**, 326–337.
- Petykiewicz, J. (1992). *Wave Optics*. Warsaw: Polish Scientific Publishers.
- Ramachandran, G. N. & Ramaseshan, S. (1961). *Crystal Optics*. Berlin: Springer.
- Shuvaeva, V. A., Glazer, A. M. & Zekria, D. (2005). *J. Phys. Condens. Matter*, **17**, 5709–5723.
- Tixier, T., Heppenstall-Butler, M. & Terentjev, E. M. (2005). *Eur. Phys. J. E*, **18**, 417–423.
- Wahlstrom, E. E. (1960). *Optical Crystallography*, 3rd ed. New York: John Wiley.
- Wenk, H.-R. & Van Houtte, P. (2004). *Rep. Prog. Phys.* **67**, 1367–1428.
- Yun, W. & Azuma, N. (1999). *Annals Glaciol.* **29**, 155–162.